Journal of
Mechanics of
Materials and Structures

Yiska Goldfeld, Till Quadflieg, Stav Ben-Aarosh and Thomas Gries

msp

■
■msp

MICRO AND MACRO CRACK SENSING
IN TRC BEAM UNDER CYCLIC LOADING

Yiska Goldfeld, Till Quadflieg, Stav Ben-Aarosh and Thomas Gries

This paper studies the ability of self-sensory carbon/glass textile reinforced concrete (TRC) beams to distinguish between micro- and macrocracking. In the proposed configuration, continuous carbon rovings knitted into the textile mesh serve both as the structural reinforcement and as the sensory system. The paper faces the challenge of detecting structural damage within the TRC structure. In this study, damage is defined as the formation of macroscopic cracks, which lead to the accumulation of significant irreversible residual deflection and to a reduction of the relative stiffness of the component. We explore experimentally the correlation between the electrical resistance change and the change of the structural properties and suggests crack detection parameters in order to identify, and mainly to distinguish, between micro- and macrostructural phenomena. Carbon rovings are found to provide electromechanical sensing capabilities, having the ability to distinguish between inner micromechanical structural phenomena and macroscopic ones. These observations are a step towards the applications of SHM techniques by intelligent carbon-based TRC elements.

1. Introduction

Multifunctional textile reinforced concrete (TRC) structures combine the advantages of high performance material and structural systems with those of integrated structural health monitoring system. The technology is based on a biaxial warp knitted fabric made of continuous fiber rovings (glass and carbon), which are embedded within thin-walled concrete structures, and serve two purposes simultaneously: reinforcement and monitoring. In this structural configuration, the textile reinforcement can easily follow a curved geometry of the structure. It also allows the reduction of wall thickness, mainly by means of the superior corrosion resistance of the reinforcement material that makes minimum concrete coverage obsolete.

TRC structures can be found in various applications such as pipes, tanks and shell like structures [Silva et al. 2011; Shams et al. 2014]. Such structures are inherently susceptible to internal or external damage such as cracks and material degradation. Yet, such structures are usually characterized by limited accessibility and inspection possibilities. Unless detected early, such damage would increase maintenance cost, disrupt operations and possibly lead to a catastrophic failure.

As opposed to reinforced concrete structural elements with steel rebar, which are allowed to be cracked during their service life, in the case of TRC structures, an adequate design allows for distributed multiple microcracks along the structures. In the latter case, due to the mechanism of the bonding and stress transfer between the concrete and the filaments in the roving, macroscopic cracks considerably degrade the reinforcement roving and reduce its load carrying capacity. The filaments of the roving that are located along the interface with the concrete (called the sleeve filaments [Bartos 1987; Zhu and Bartos 1997]) break due to the macroscopic cracking and only a reduced number of filaments that are located at

the core of the roving can further carry the loading (see, for example, [Bentur et al. 2010; Yardimci et al. 2011]). It is therefore essential to explore the damage sensing capabilities of TRC structures in order to further develop a reliable monitoring routine for early detection and rectification of structural damage.

Damage identification and structural health monitoring (SHM) techniques for reinforced concrete elements range from traditional methods such as visual inspection or tap tests, to modern techniques based on embedded or surface mounted strain sensors. The latter are either localized (such as resistor strain gauges and fiber Bragg grating) or distributed (such as time domain reflectometry in fiber optics; see, for example, [Khotiaintsev et al. 2013; Klar et al. 2010; Goldfeld and Klar 2013; Antunes et al. 2011; Majumder et al. 2008; Li et al. 2004; Lee 2003]). In the context of sensory TRC elements, there is a range of research works reporting on the implementation of the sensory devices in the textile grid, such as optic fibers (e.g., [Krebber et al. 2012; Montanini et al. 2012]). These methods are usually based on implementing the sensing system in a structural element, which requires physical accommodation in the load-bearing element. The potential degradation of the effective properties of the host element, and the clear distinction between the structural system and the sensory one (which is not a part of the load bearing system) are drawbacks of this approach. Also, stemming from the concept of joining two separate systems together, the interface between the structural and the sensory systems and the corresponding ability to maintain a coordinated action of the two are potential weak aspects. Finally, the sensory system itself is commonly expensive and its implementation is costly, time-consuming, and it requires specially trained personnel.

Using hybrid carbon fiber textiles as reinforcement for a TRC element and utilizing the electrostructural characteristics of the carbon rovings as a basis for its sensory feature offers a preferred alternative that overcomes some of the aforementioned drawbacks. The sensory TRC element is based on using the same array of continuous carbon rovings for the reinforcement required for the load resisting system and, at the same time, using them as the component providing the structure with the self-sensory feature. For the case of glass/carbon textile configurations, some carbon rovings replace glass fiber rovings and they are embedded in a glass textile grid as part of the production process of the textile. The implementation of the textile in the concrete element is a straightforward act, which is not different than the production process of standard textile reinforcement within TRC elements. The self-sensing capacity of the sensory textile is gained by correlating between the electrical response of the carbon rovings and the structural response of the TRC element. Therefore, the cost and labor inputs needed for converting the standard TRC component into a sensory one are almost eliminated.

Studies on the use of the electrical conductivity features of carbon fibers for sensing purposes can be found in the literature; see, for example, [Chen and Chung 1993; McCarter et al. 2007; Vaidya and Allouche 2011; Wang and Chung 1996; Christner et al. 2012; Horoschenkoff and Christner 2012; Angelidis et al. 2004; Todoroki and Yoshida 2004; Wen and Chung 1999; Wen et al. 2000; Goldfeld et al. 2016a; 2016b; Quadflieg et al. 2016]. There is a clear distinction between strain sensing and damage sensing. Strain can be reversible and it is generally monitored within the linear elastic regime of the structure. Therefore, it is not necessarily accompanied by macroscopic cracks or damage. While in the case of damage sensing, the mechanism of the electrical response is inherently different. Damage leads to an irreversible change in the electrical resistance. The more severe the damage is, the greater the irreversible component of the electrical resistance becomes. The hypothesis of this study is that the irreversibility of the electrical resistance can be correlated to the structural health. The goal is therefore to correlate between the electrical response and the structural health. Understanding the correlation in

the damaged regime is essential for the development of intelligent carbon-based TRC structural elements with inherent SHM capabilities in the future.

The piezoresistivity (the effect of strain on the resistivity) of short carbon fibers embedded in a cement matrix has been extensively investigated in the literature (see, for example, [Chen and Chung 1993; McCarter et al. 2007; Vaidya and Allouche 2011]). The carbon fibers in such applications are an additive for rendering detectable piezoresistive properties to the concrete mixture by improving the electrical conductivity of the cast concrete element. Therefore, in this case, the fibers are not the sensor itself.

An alternative sensing concept is obtained by detecting changes to the electrical resistivity of continuous carbon rovings. In this case, the carbon rovings, made of thousands of carbon filaments, serve both as the structural reinforcement and as the sensory agent. The sensory capability is obtained by monitoring changes to the electrical resistance of the roving due to straining. Investigations of this concept were mainly focused on carbon-based polymer or epoxy matrix composites (see, for example, [Wang and Chung 1996; Christner et al. 2012; Horoschenkoff and Christner 2012; Angelidis et al. 2004; Todoroki and Yoshida 2004]). Relatively few studies have investigated the piezoresistivity effect of continuous carbon fiber embedded in a cement matrix. Wen and Chung [1999] and Wen et al. [2000] investigated the correlation of the changes to the electrical resistance with the straining of a continuous carbon fiber embedded in cement paste under uniaxial tension. They concluded that the electrical resistance increases upon tension and that the electrical resistance increase is mostly reversible. Goldfeld et al. [2016a; 2016b] investigated the piezoresistive effect of hybrid glass/carbon TRC beam elements under monotonic loading and under cyclic loading, respectively. These two studies moved from the fundamental single roving or bundle of fibers scale to the integrative TRC structural element scale. It was reported that along the linear-elastic regime, the integrative electrical resistance can be correlated to the distributed strain, and since the electrical resistance is mostly reversible, a gauge factor can be defined. Slight irreversibility was attributed to inner irreversible micromechanical processes, such as degradation of the fiber-concrete bond strength and breakage of single filaments [Banholzer and Brameshuber 2004; Banholzer et al. 2006; Bentur et al. 2010; Yardimci et al. 2011].

Damage sensing, which differs from strain sensing, is essential in the case of thin walled TRC structures. It has been mainly reported for the case of short carbon-based cement composites; see, for example, [Wen and Chung 2007; Ding et al. 2013; Teomete 2015; Meehan et al. 2010; Yao et al. 2003; Peled et al. 2001; Bontea et al. 2000; Reza et al. 2003]. In the case of damage sensing, the mechanism of the electrical response is different. Damage leads to irreversible changes in the electrical resistance, depending on the severity of the damage [Bontea et al. 2000; Reza et al. 2003].

In the case of damage sensing with continuous carbon fibers, most of the studies were focused on carbon fiber reinforced polymers; see, for example, [Wang and Chung 2006; Chung 2007]. In these studies, it was reported that the accumulation of damage and irreversible structural response triggered irreversible changes to resistance.

Studies on damage sensing with continuous carbon rovings embedded in concrete elements were only focused on the correlation between internal microstructural phenomena, such as the degradation of the interface between the fiber and the concrete matrix, and the measured electrical resistance; see [Wen and Chung 1999; Wen et al. 2000; Goldfeld et al. 2016a]. These microstructural phenomena characterize the linear-elastic regime of the response, which is considered as the healthy state of the structure and therefore is attributed to the strain sensing. Damage sensing, which extends beyond the

aforementioned strain sensing concepts is, on the other hand, the most crucial monitoring capability of thin-walled TRC structures. The goal of the current study is therefore to investigate the structural and the electrical response of a damaged TRC element. As opposed to [Goldfeld et al. 2016a], which focused on the piezoresistive behavior of the carbon-based textile along the linear-elastic regime, the present study focuses on the essential capabilities of the carbon-based textile to sense structural damage in terms of macroscopic crack and to quantitatively distinguish between micro- and macrostructural phenomena. The goal is therefore to explore and characterize the correlation between the structural and electrical responses of a TRC beam before and after cracking.

In this study, the damage state is defined by the formation of a macroscopic crack. In TRC composites, since the reinforcing rovings are made of thousands of filaments, the bonding and stress mechanism between the filaments and concrete matrix play a significant role in the load carrying capacity of the roving and, as a result, of the whole component. Due to increased tension loading, and after formation of the first matrix crack, the sleeve filaments of the roving break and filaments in the core of the roving can further carry on the increasing load providing strain hardening behavior. It is commonly modeled by a telescopic pull-out mechanism (see, for example, [Bartos 1987; Zhu and Bartos 1997; Bentur et al. 2010; Yardimci et al. 2011]) with microcracks being smaller than 100 microns in width during the strain hardening stage, where significant load can be transferred across the microcrack. Therefore, an adequate design allows for distributed multiple microcracks along the structures to be considered here as being in the healthy state. When a macrocrack opens, at the cracked zone all sleeve filaments break, including progressive breakage of core filaments, as well as extensive displacement in the core filaments, leading to a significant reduction in the load carrying capacity. Thus, as a result of the widening of one (or several) of the microcracks into a macrocrack (significantly wider than 100 microns), the strain hardening behavior turns into a marked softening one, with significant reduction in the load bearing capacity of the TRC component. The formation of the macrocrack can be seen by a drop of the load-deflection curve, as in the present study. Therefore, the formation of a macrocrack is defined as the damaged state in this study.

The hypothesis of this study claims that the micro- and macrostructural response are reflected by the measured electrical response of the carbon rovings. Therefore, the goal is to correlate between the structural response and the electrical measure, and consequently estimate the structural health.

In order to support the hypothesis of the study, the structural and electrical response of a TRC beam are experimentally investigated under cyclic loading at the healthy and at the cracked state. The loading cycles extend the predamaged loading process presented in [Goldfeld et al. 2016a] to the damaged cracked-state. For the sake of completeness, the relevant data from [Goldfeld et al. 2016a] are shortly presented. The preliminary information regarding the structural and electrical setups is mentioned here again, and selected results for the healthy state are presented as a reference in order to compare, distinguish and highlight the differences between the strain and damage sensing capabilities of the carbon rovings.

2. Experimental investigation

The experimental investigation focuses on the crack sensing capabilities of the carbon rovings. It uses the cyclic loading test conducted in [Goldfeld et al. 2016a] in the precracked range as reference and extends the cyclic loading to the cracked regime. The generic setups and properties of the sensory textile, the beam sample, the electrical layout, the testing scheme and the procedure for the compensation for the effect of the temperature on the sensing system are presented in [Goldfeld et al. 2016a], and (for clarity

and completeness) will be briefly presented here. In the previous work, the strain sensing capability at the healthy state was investigated, while the current study focuses on the structural and the sensing responses of the beam at the cracked regime.

2.1. *Sensory textiles.* The sensory textile is based on two types of rovings: rovings made of glass, which are the main reinforcement platform, and rovings made of carbon, which are also used as the sensory system (see also [Goldfeld et al. 2016a; 2016b]); see Figure 1. The material properties of the glass and the carbon rovings are given in Table 1.

The reinforcing textile structure consists of a warp-knitted grid of alkali-resistant (AR) glass rovings and sensory carbon rovings, which are spaced 7–8 mm from each other. The weft direction consists only
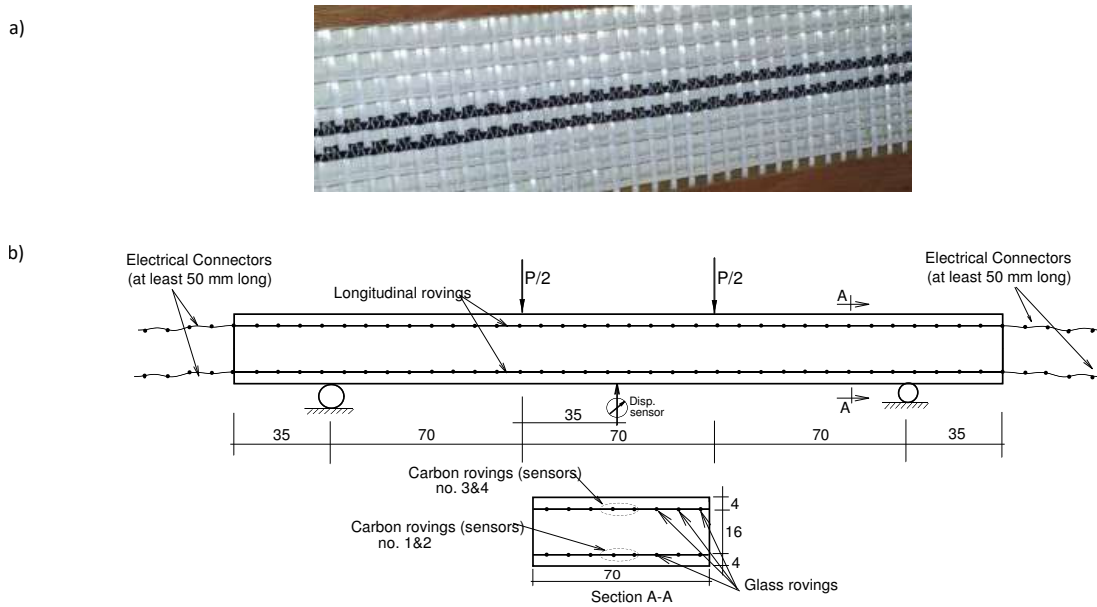

Figure 1. (a) The reinforcement sensory textile; (b) schematic drawing, cross section, geometrical parameters and loading scheme of the TRC specimen (dimensions in mm) [Goldfeld et al. 2016a].

	glass roving	carbon roving
density [tex]	2400	3300
specific mass density [kg/m^3]	2680	1800
modulus of elasticity [GPa]	72	240
filament tensile strength [MPa]	1700 (elongation 2.4%)	4000 (elongation 1.7%)
filament diameter [μm]	19	7
filament count	–	50000
equivalent cross-sectional area [mm^2]	0.9	1.81
electrical resistance [Ω/m]	∞	13

Table 1. Material properties of the glass and the carbon rovings.

of AR glass rovings. In the warp direction, some of AR-glass rovings were replaced by sensory carbon rovings in a symmetric layout. Placing the carbon rovings only in one direction avoids potential electrical linking between perpendicular rovings, but limits the sensing capabilities to one chosen direction. The rovings are knitted with warp-knitting yarns made of polypropylene. The type of knitting stitch is pillar; its influence on the tensile properties of the roving within the concrete has been investigated in [Stolyarov et al. 2015a]. The cross-sectional area of the rovings as given in Table 1 is a theoretical value and relates to the cross section of all filaments counted together and is used for the stress calculation. The cross section and occupied space of the roving is much bigger, due to the spaces between the filaments. The shape of the roving cross section also depends in the stitch type, e.g., pillar stitch forms a more circular shaped cross section, while the tricot stitch forms a more elliptical shaped cross section; see [Stolyarov et al. 2015b]. The textile used had a roving width of 1–2 mm. The production of the glass/carbon textile uses a conventional process with no specific or special treatment of the textile. The electrical integration of the carbon fiber rovings into the data acquisition (DAQ) system uses a cast connector, made of conductive epoxy, at the ends of each carbon roving; see [Goldfeld et al. 2016a].

2.2. *TRC beam samples.* Beam samples reinforced with the glass/carbon textile have been designed and manufactured. The specimens are 280 mm long, 70 mm wide and 24 mm thick, according to the loading setup used in this research (four point bending), and they were reinforced with two layers of the sensory textile located 4 mm from the upper and lower faces of the element. The thickness was determined in order to capture both microstructural behavior (so it should not be too thick), as well as macrostructural behavior (so it should not be too thin). Therefore, the distance between the textiles is determined as 16 mm, and the total thickness of the beams is 24 mm. The width (70 mm) is determined according to the textile grid (the interval between the rovings is about 7 mm–8 mm). The carbon rovings are located at the middle of the beam and the influence of the added stiffness of the carbon rovings with respect to the glass rovings can be averaged along the beam width. The length of the beam (280 mm) is determined in accordance to the loading scheme and the estimated bending capacity of the beam's cross section.

Each textile layer includes six longitudinal (0°) glass rovings and two longitudinal carbon rovings. The transverse (90°) rovings are all made of glass fibers; see Figure 1. Special molds were developed in attempt to maintain a preliminary low level of pretensioning in all four directions to both layers of the sensory smart textile. The pretensioning was performed manually; see [Goldfeld et al. 2016a]. In Figure 1, the layout of the beam and its cross sectional properties are given.

A commercial grout mixture (Sika Grout 214) was used for the concrete matrix, which was prepared with a water per dry material ratio of 0.125. The concrete matrix was not modified with any electrical conductive component and therefore is considered as an isolating dielectric. The TRC beams were cured at room temperature for 48 hours. According to EN 196-1:2005, after 28 days, the tensile strength and the compression strength of the grout were determined. The mean values $\pm$ standard deviation are $f_t = 11.71 \pm 0.49$ MPa and $f_c = 66.9 \pm 2.77$ MPa.

2.3. *Sensing concept.* The hypothesis of this study is that the measured electrical change of the carbon rovings embedded in the concrete beam has the capabilities to distinguish between internal microstructural phenomena and macroscopic ones. In particular, it aims to explore the correlation of the electrostructural response to the evaluation of damage.

In the examined layout, the bending moment diagram is not constant and thus the stress as well as the damage are not uniformly distributed along the roving. This becomes particularly critical after the formation of the macroscopic crack. On the other hand, the measured electrical resistance is integrally attributed to the entire roving monitored from one end to another. Thus, the measured electrical resistance along each roving is considered as an integrative index. This means that only an integrative value of the electrical resistance R_x and resistance change ΔR can be evaluated. The integrative electrical resistance of the roving is given in an integral form, (see also [Goldfeld et al. 2016a]):

$$R_x = \int_0^L r(x)\,\mathrm{d}x, \tag{1}$$

where $r(x)$ represents the electrical resistance per unit length depending on the strain distribution, the damage distribution and on the temperature change, and L is the length of the beam. Consequently, the resistance change ΔR due to damage can be defined by

$$\Delta R^{\mathrm{measured}} = (R_x^{\mathrm{damage}} - R_x^0) + \Delta R_x^{\mathrm{temperature}} = \int_0^L r(f(\varepsilon(x), \mathrm{damage}(x)))\,\mathrm{d}x - R_x^0 + \int_0^L r(\Delta T)\,\mathrm{d}x. \tag{2}$$

In the above equations, $\varepsilon(x)$ designates the distribution of the strain. In the case of a healthy state it depends exclusively on the loading scheme and the moment distribution. At the damaged state, $\varepsilon(x)$ is also influenced by the location and severity of the damage along the structure, especially in statically indeterminate structures. The function damage(x) designates the distribution of the damage along the structures. Therefore, $r(f(\varepsilon(x), \mathrm{damage}(x)))$ is the electrical resistance along the roving, which is both strain and damage dependent, and $r(\Delta T)$ is the distributed resistance due to temperature change. In the current study, it is assumed that there is no coupling between the temperature and structural effects. Therefore, in order to correlate the electrical resistance change to the structural response, linear temperature compensation is performed; further details are given in Section 2.5. R_x^0 is the reference electrical resistance, measured before the mechanical loading was applied. The damage sensing capabilities can be performed by comparing the electrical resistance at the healthy state damage$(x) = 0$ and at the damaged state damage(x), or by comparing the electrical resistance change at a specific unknown state before $\varepsilon(x) = 0$ and after loading $\varepsilon(x)$. Both possibilities are discussed in Section 3.3 by means of crack detection parameters.

From the structural point of view, the distinction between strain sensing and damage sensing is governed by the micromechanism of the structural response, which is characterized by the bonding mechanism of the roving and the concrete matrix. A simplified constitutive model of the stress-strain diagram of TRC structures is presented in Figure 2 (see [Mobasher et al. 2014]). The constitutive model of the roving under internal tensioned loading (Figure 2a) is characterized by a linear strain-stress relationship up to the macroscopic cracking strain ε_{cr}. This part can be represented by the tensile stiffness E. Along this phase multiple microcracks are formed. Then, after the formation of a macroscopic crack, a postcracking modulus E_{cr} can be defined. E_{cr} is lower than E and its sign depends whether strain softening or strain hardening characterize the postcracking response. The reduction in the elastic modulus is due to the breakage of all sleeve filaments at the cracked zone (see, for example, [Bartos 1987; Zhu and Bartos 1997; Bentur et al. 2010; Yardimci et al. 2011]). Along the last phase, only the core filaments within the rovings are able to carry the tensioned load along the structure, which can be represented by a constant
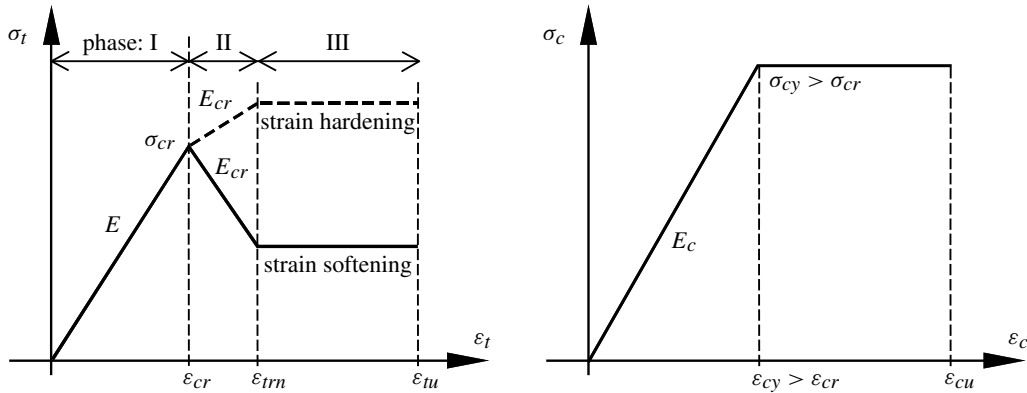
Figure 2. Fiber reinforced concrete model: left, tension model; right, compression model; according to [Mobasher et al. 2014].

lower tensile strength and perfectly plastic behavior, phase III in Figure 2a. In the compression model (Figure 2b), the stress increases linearly up to the yield strain ε_{cy}, and then remains perfectly plastic. In the current study it is assumed that the strain sensing is represented by the first phase (indicated in Figure 2). This phase is characterized by internal microstructural process associated to the slight degradation of the bonding mechanism and therefore by generally linear-elastic behavior. The damage sensing, on the other hand, is attributed to the second and third phases, after a macrocrack has been formed and only the core filaments within the roving carry on the load. The hypothesis is that both phases, the pre- and postcracking, are reflected by the measured electrical resistance.

The inevitable shift from the distributed effect reflected by changes to $r(f(\varepsilon(x), \text{damage}(x)))$ and the integrative one reflected by changes in R_x (equations (1) and (2)) establishes the ability to identify structural events but eliminates the ability to identify its exact location along the roving. Moreover, distributed small cracks and one severe crack can eventually lead to the same integrative electrical measure. This means that the exact location of the damage and its pattern cannot be identified by the integrative measure but only its overall effect in terms of global-integrative indexes. This drawback can be handled by using various approaches (e.g., segmentation of the TRC elements), which are beyond the scope of the present paper. Nevertheless, the study will demonstrate the capability of the integrative electrical resistance to clearly distinguish between a healthy state and a damaged state (after cracking has been formed).

The measurement methodology takes advantage of the continuous configuration of the carbon rovings within each structural segment. Following the experimental setup outlined in detail in [Goldfeld et al. 2016a; 2016b], the electrical setup uses a Wheatstone bridge scheme; the general layout is illustrated in Figure 3. In this configuration, the carbon roving is serially implemented along with the external resistor in the bridge and the voltage change across the bridge is measured. Since the properties of all other resistors are known, and since only the carbon roving triggers the bridge out of balance, the voltage change across the bridge can be converted into changes to the integrated electrical resistance of the carbon fiber roving, R_x as follows:

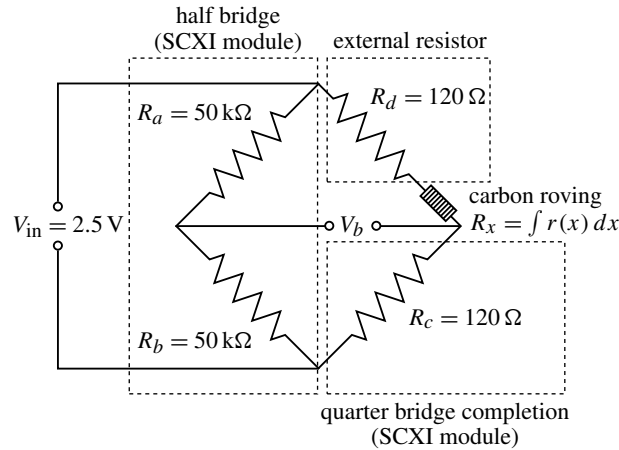$$R_x = \frac{V_{\text{in}} R_c}{V_b + \alpha V_{\text{in}}} - R_c - R_d, \tag{3}$$

Figure 3. Wheatstone bridge circuit setup (generic setup); see also [Goldfeld et al. 2016a]. (R_x designate the resistance of the carbon roving, V_b is the measured voltage.)

where V_{in} is the excitation voltage, V_b is the signal voltage, $\alpha = R_b/(R_a + R_b)$, and R_a, R_b, R_c and R_d are known resistors.

In order to measure the resistance according to the above methodology, carbon rovings were connected to a National Instruments (NI) signal conditioning module (NI-SCXI-1521B) installed in a NI-SCXI-1000 chassis; see Figure 3. The data acquisition system (DAQ) is NI-USB-6361. Therefore, the resistance of the resistors of half of the bridge, which are an integrated part of the SCXI module, are $R_a = R_b = 50\,\text{k}\Omega$, the resistance of the resistor of the quarter bridge completion, which is also an integrated part of the module, is $R_c = 120\,\Omega$; the external resistor is therefore determined to be $R_d = 120\,\Omega$ (VISHAY PTF56120R00BZEK), and thus $\alpha = 0.5$ and $V_{\text{in}} = 2.5\,\text{V}$. The DAQ system has 24 channels, which allows simultaneous measurement of all four rovings within the loaded beam as well as the one of the carbon roving within the reference beam (used for the temperature compensation, see Section 2.5).

Due to the resistance of the carbon roving R_x, which is approximately $3.1\,\Omega$ before the loading process, the bridge is not balanced. The initial base value is therefore $V_b = 20\,\text{mV}$. In the presented configuration, the maximum change to V_b was measured as $50\,\mu\text{V}$ corresponding to a change of $9.6\,\text{m}\Omega$ in the resistance of the carbon roving.

2.4. *Loading and external monitoring.* The experimental investigation is based on the cyclic loading of TRC beam samples. The mechanical testing uses the cyclic testing scheme presented in [Goldfeld et al. 2016a] and extends the loading and the response to the damaged regime. As opposed to the previous work, which focused on the piezoresistive behavior of the carbon-based textile along the linear-elastic regime, the present study focuses on the essential capabilities of the carbon-based textile to sense structural damage in terms of a macroscopic crack. In order to compare, distinguish and characterize the electrostructural response before and after cracking, the structural response at the healthy state [Goldfeld et al. 2016a] is presented here as a reference.

The mechanical testing of the beam was conducted in a displacement control mode. The beam was tested under a four-points flexural bending scheme with span lengths of 70 mm and 210 mm between loading and supporting, respectively; see Figure 1. In order to examine the ability of the sensory carbon rovings to monitor damage, the first five loading cycles were conducted along the healthy state (see
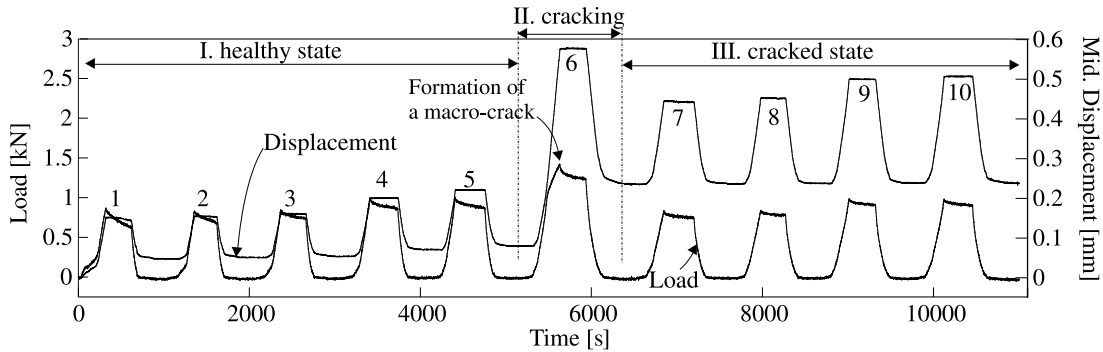
Figure 4. Ten load cycles of the TRC beam: load and displacement measured at the middle of the beam vs. time. The healthy state data is from [Goldfeld et al. 2016a].
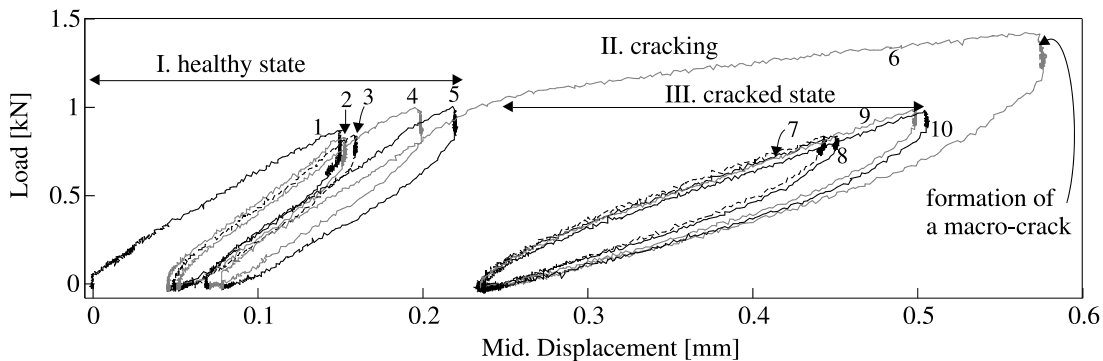

Figure 5. Load versus displacement (along the ten loading cycles). Healthy state data is from [Goldfeld et al. 2016a].

the discussion in [Goldfeld et al. 2016a]). Then, an additional loading cycle was conducted up to the formation of macrocracking, which was indicated by a drop in the measured load. Finally, four additional loading cycles were conducted at lower load levels. All loading cycles were conducted under a uniform loading, unloading and reloading rate of 0.1 mm/min.

The test setup also includes monitoring the load, the crosshead movement and the vertical displacement at the middle of the beam. The load and the displacement versus time curves appear in Figure 4, and the load versus prescribed displacement curves are shown in Figure 5. The loading pattern includes ten loading cycles. The load for cycles 1–3 was 0.85 kN, and the load for loading cycles 4–5 was 1 kN. Additional details of these first five loading cycles, which corresponded to a healthy state of the TRC beam, are given in [Goldfeld et al. 2016a]. The load level of the sixth loading cycle was determined by the formation of the macroscopic flexural crack, indicated by a drop in the measured load. It was observed at a load level of 1.25 kN; see Figures 4 and 5. After the experiment was terminated and the beam was removed from the loading machine, the width of the crack was measured to be about 0.25 mm.

Therefore, the first three loading cycles refer to load levels that are about 68% of the cracking load, and the next three loading cycles refer to load levels that are about 80% of the cracking load. Then, four additional loading cycles were applied. Two (loading cycles 7–8) at a load level of 68% of the cracking
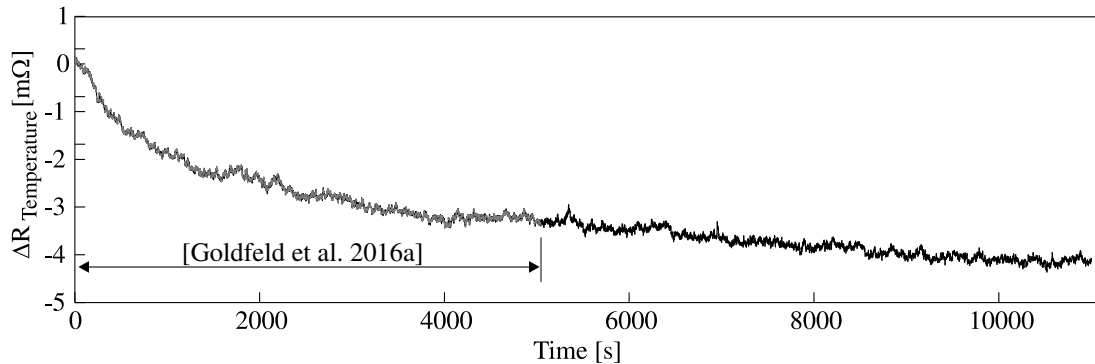
Figure 6. Resistance change of the sensory carbon roving embedded in the unloaded reference beam vs. time (up to $t = 5200$ s; see [Goldfeld et al. 2016a]).

load and two (loading cycles 9–10) at a load level of 80% of the cracking load. These four loading cycles are the ones that will be attributed to the detection procedure.

Selecting the same mechanical pattern of loading-unloading-reloading at the healthy state and at the damaged state is motivated by several aspects. First, the phase of loading and then holding the displacement for 4–5 minutes, for related loading cycles, aims to examine the scenario of exposing the structure to a short term low load level, which is considered to be the monitoring load level for the damage identification procedure. The selected pattern is not intended to trigger and detect long term time dependent behavior, but it can shed light on the short term relaxation effects at the healthy and at the damaged regimes. This is relevant to the sustained loading period as well as to the period between one loading cycle, and another and it aims to simulate a real monitoring scenario. Second, it aims to compare the response at the healthy state and at the damaged state. Choosing the same pattern of loading cycles before and after damage enables the comparison of structural and electrical responses, therefore determining whether damage has occurred and to what extent. Third, it enables the correlation of the electrical response and the load-deflection response, and thus allowing the investigation of the repeatability of the electrical measure with respect to the structural health, and the possible evolution of irrecoverable processes at the damaged state.

2.5. *Temperature compensation.* Parallel to the effect of the mechanical-structural behavior, a change in temperature also triggers changes to the electrical resistance of the carbon rovings. It was reported that as the temperature increases, the resistance of the carbon fiber decreases [Xu et al. 2011; Wen et al. 1999; Crasto and Kim 1993; Yang et al. 2009]. Since the carbon rovings are exposed to a continuous electrical current, the temperature of the rovings increases, leading to resistance change. Therefore, temperature compensation should be performed in order to exclusively correlate the structural response and the measured resistance. In this study, the resistance change due to temperature is measured by a carbon roving embedded in a reference TRC beam (identical to the examined beam) which is not subjected to a mechanical load. Both beams (the loaded beam and the reference beam) were connected to the same DAQ system, and the voltage change in the reference beam was simultaneously measured along the entire process; see [Goldfeld et al. 2016a]. The electrical resistance change in the reference beam is given in Figure 6. It is solely attributed to the temperature effect, and it is subtracted from the response of

the beam subjected to the mechanical loading. Note that Figure 6 extends the results given in [Goldfeld et al. 2016a] beyond the healthy state of the loaded beam (from about $t = 5200$ s) to the damage state.

3. Results and discussion

3.1. *Structural response and temperature effect.* The structural behavior for all loading cycles (healthy and damaged) is presented in Figures 4 and 5, and the effect of temperature on the electrical resistance is presented in Figure 6. The residual displacement at the end of each load cycle and the relative stiffness, calculated by the change of the measured load per unit deflection and represented by the slope of the loading branches in Figure 5, for each load cycle are summarized in Table 2.

The first macroscopic visible flexural crack was detected at a load level of 1.25 kN at the sixth load cycle (indicated in Figures 4 and 5). It is reflected by a drop in the measured load and by a gradual residual deflection, as can be seen in Figures 4 and 5 and Table 2. A picture of the beam with its macroscopic crack (of about 0.25 mm width) is given in Figure 7. The picture was taken after the experiment was terminated and the beam was removed from the loading machine. It should be noted that this is the only visible macrocrack that was detected. The lower strain gauge which appears in the figure, and used in [Goldfeld et al. 2016a], was broken due to the cracking. Immediately after detecting the formation of the crack, the displacement was held for 300 s. The next loading cycles mimic the loading cycles of the healthy state. Usually for structural health monitoring purposes, the load level used is much lower than the load level that actually causes the damage. In the present study, the load levels are the same as the ones applied at the healthy state, although it is relatively high for monitoring purposes. Choosing the same load level for the damaged and for the healthy states enables us to investigate and compare the structural and the electrical responses of the TRC beam, and therefore characterize the discrepancies in terms of damage sensing parameters.

Based on the load and displacement results, the structural response can be divided into three main states. The first one (cycles 1–5) corresponds to the generally linear-elastic state. It was thoroughly investigated in [Goldfeld et al. 2016a] and is considered here again to reference the structural and electrical response of the damaged state. The second state (sixth cycle) corresponds to the cracking load. The third state (cycles 7–10) corresponds to the cracked-damaged structural behavior of the beam. The three states are indicated in Figures 4 and 5.

The structural response of the first state is characterized by a linear-elastic behavior with a negligible level of hysteresis. The load is slightly relaxed under the prescribed displacement and a small gradual residual deflection is accumulated after each load cycle (see also Figure 5 and Table 2). This is an outcome of internal microstructural phenomena related to the interaction between the concrete mixture and the

	healthy state (I)					cracking	cracked state (III)			
loading cycle	1	2	3	4	5	6	7	8	9	10
residual displacement [mm]	0.046	0.049	0.052	0.069	0.079	0.234	0.234	0.237	0.237	0.237
relative stiffness [kN/m]	5531	7553	7316	6761	6373	6058	3627	3695	3491	3404

Table 2. Residual displacements and relative stiffness measured at the end of each loading cycle.

textile mesh [Bentur et al. 2010; Yardimci et al. 2011; Banholzer and Brameshuber 2004; Banholzer et al. 2006] and especially to the degradation and breakage of the outer filaments of the rovings.

Since the response of the first cycle of the healthy state is different from the next four cycles, and is mainly due to the initial part of the loading that is attributed to the settlement and the slight self-organization of the test setup [Goldfeld et al. 2016a], it is not considered in the following discussion.

The sixth loading cycle, the second state, defines the formation of multiple microcracks along the loading brunch. The loading phase of this cycle ends with a gradual load drop as a result of the widening of one (or several) of these microcracks (formation of a macrocrack), indicated in Figures 4 and 5. Due to that, the entire filament of the roving along the interface with the concrete matrix at the cracking zone breaks, which leads to irreversible gradual deflection and to lower stiffness. Once there was indication of formation of the macrocrack, the displacement was held for about 4–5 minutes and then unloaded.

After the formation of the macroscopic crack, the loading cycles of the third state (cycles 7–10) are characterized by a new linear-elastic state and the global response is governed by the macroscopic crack. The structural behavior is linear with almost no hysteresis, load relaxation or accumulation of additional gradual deflection. In spite of the relatively high levels of load after damage (68% and 80% of the cracking load), the four cycles at the damaged state reveal a repetitive pattern. It is reflected by the load-deflection curve (Figure 5) as well. This state is characterized by a lower and consistent slope of the loading brunches compared to the healthy state (Table 2), which corresponds to the new relative stiffness of the TRC beam. The reduced stiffness is an outcome of the presence of the macroscopic crack and its consistent pattern is related to the new linear state. These phenomena define quantitative indicators for the accumulation of mechanical damage in the beam. Furthermore, it enables one to distinguish between reversible microstructural phenomena to irreversible macroscopic ones, which is reflected by the electrical response of the new state. It also allows us to consider loading cycles 7–10 as the monitoring loading cycles (i.e., the cycles that are of interest), even though they were conducted at a relatively high load level with respect to the cracking load.

Another aspect that supports the consistent and repeatable structural response in the damaged state is the residual deflection after each cycle; see Table 2. After the sixth load cycle, the residual deflection measured at the middle of the beam increases from 0.079 mm (at the end of the first state) to 0.234 mm
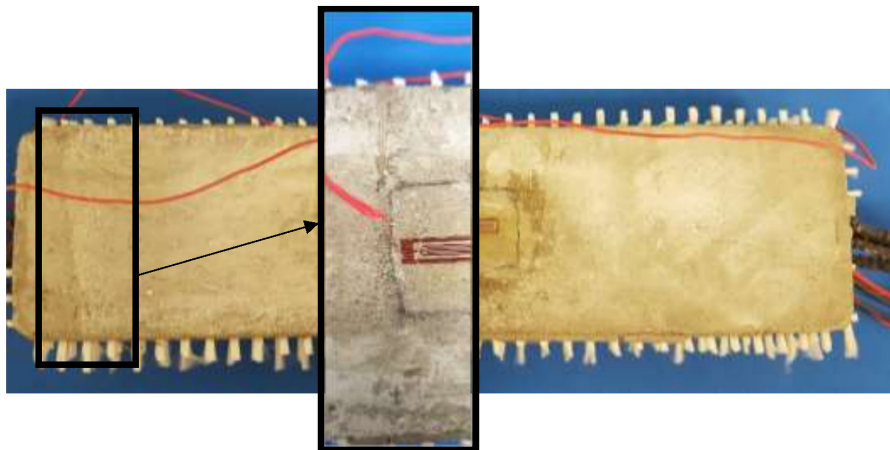

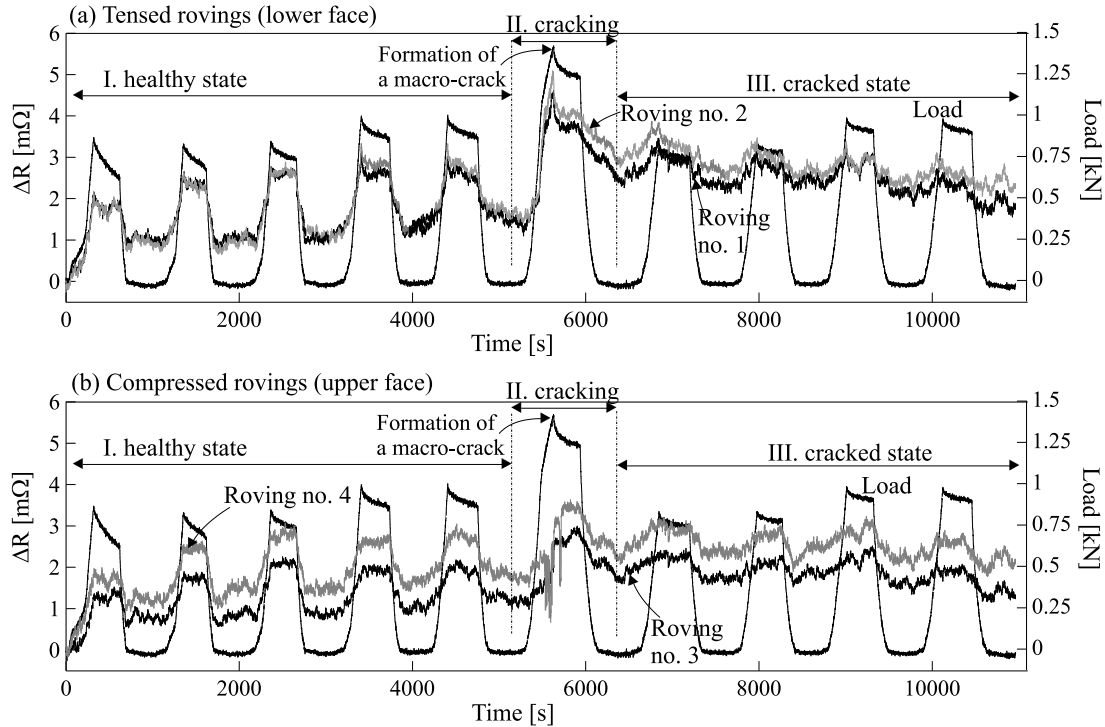**Figure 7.** Picture of the cracked TRC beam.

Figure 8. Resistance change (after temperature compensation) of the sensory carbon rovings of the loaded beam vs. time. Initial resistance $R_0 = 3.1\,\Omega$. Healthy state data is from [Goldfeld et al. 2016a].

(after cracking). This value remains almost constant after each of the last four cycles. Before cracking, the mechanical behavior is characterized by the microstructural mechanism of the bonding between the textile and the concrete matrix. After cracking, the structural response is completely different and it is governed by the mechanism of the macroscopic crack. Any additional internal microstructural process, if occurred, has almost no effect on the global structural response. The macrostructural response at the damaged state is repeatable as reflected by the constant residual deflection after each loading cycle and is more consistent compared to the response at the healthy state. The gradual residual deflection and its consistent values can define another quantitative indicator for the accumulation of mechanical damage in the TRC beam.

3.2. *Sensing micro- and macrocracks.* In order to support the hypothesis of this study, the sensing capabilities of the carbon rovings is first demonstrated. The sensing methodology and the associated crack detection approach focus on the electrical response due to mechanical loading before and after a macrocrack has formed. The changes to the electrical resistance of the carbon rovings during all ten loading cycles are plotted versus time in Figure 8. The results were temperature compensated using the results outlined in Figure 6. The results for the two tensed rovings (1 and 2) are presented in Figure 8a and those for the two compressed rovings (3 and 4) are presented in Figure 8b.

The reference electrical resistance of the rovings before the loading process was approximately 3.1 Ω. The resistance change was measured with respect to this value. The averaged initial resistance values R_x^0 for each load cycle (for the healthy state and for the damage state) are given in Table 3. It is taken as the average measured resistance along the unloaded phase before each loading cycle. Note that the actual electrical resistance along the roving is the reference resistance (3.1 Ω) plus the resistance given in Table 3.

The curves and the results outlined in Figure 8 and Table 3 highlight several observations regarding the sensing capabilities of the carbon rovings along both the healthy and the damage regimes:

(1) It reveals a clear correlation between the electrical readings of the rovings (Figure 8) and the structural response of the beam (Figures 4 and 5). The sensory system is repeatable and characterized by a generally constant quality of the readings along all ten loading cycles. Even after the formation of the macroscopic crack, the electrical readings of the rovings still reflect a sound sensory capability.

(2) It implies that along all loading cycles the correlation is relatively linear. In terms of its mathematical representation, only a shift of the reference values and a linear scaling are needed in order to correlate between the structural and the electrical response.

(3) It reveals that the electrical response of the tensed and of the compressed rovings is generally repeatable along the entire loading process. It is observed that the readings of the two independent rovings located at the same height (rovings 1 and 2 in Figure 8a and rovings 3 and 4 in Figure 8b) are very similar. The constant difference between the compressed rovings was attributed to the initial loading phase of the first load cycle [Goldfeld et al. 2016a].

(4) It reveals that the electrical resistance increases also when the rovings are compressed. This issue has been discussed in [Goldfeld et al. 2016a] for the linear-elastic state (state I). The negative correlation of the compressed rovings is consistent for the healthy and the cracked state. A dimensional change without a resistivity change would have caused R_x to decrease under compression. In contrast, R_x increases. The reason for the increase in resistance, and as a result, to the negative correlation, is attributed to changes to the specific resistivity ρ at the roving level rather than to dimensional changes. For strain sensing [Goldfeld et al. 2016a] it was assumed that since each carbon roving is comprised of a large number of filaments (about 50000), under compression, the fiber to fiber interface degrades as the bundle of fibers slightly separates. In addition, the inner fibers, which are not sufficiently supported by the cement matrix or by the fiber to fiber contact stresses, are expected to be mostly affected by the compressive stresses. The latter may increase the misalignment of the fibers, cause localized rotation and deviation from the roving's axis, and even cause localized buckling of the fibers. Therefore, it was assumed that all the above phenomena eventually yield an increase in the specific resistivity at the roving level. Regardless of the dimensional changes, these effects increase the overall electrical resistance, and yield an increase in resistance under compressive loading growth and to a negative correlation. The above hypothesis is also supported by the observation that the negative correlation is stable along the entire load cycle for all loading cycles (healthy and cracked states).

(5) An interesting observation is related to the electrical resistance change at the moment when the macrocrack is formed. The structural response is characterized by a drop of the measured load and the electrical response is characterized by a rapid reduction with several oscillations of the resistance. It is observed at the tensed rovings and at the compressed rovings; see Figure 8.

The above observations clearly demonstrate the sensing capabilities of the carbon roving at the linear-elastic state of the beam, as well as at the damaged state of the beam, which is associated to the formation of cracking. The comparison between the electrical response of the carbon rovings before the formation of the cracks and their responses after the formation of the cracks reveals the following observations:

(1) It is observed that in the cracked state the measured electrical resistance is relatively high compared to the healthy state. After the accumulation of the macroscopic crack at the sixth loading cycle, the measured electrical resistance increases significantly, and the increase is irreversible. It is mainly visible at the unloaded state at the beginning of each load cycle; see Table 3. This observation is in good agreement with the structural responses due to the formation of the macroscopic crack and is correlated well to the irreversible residual deflection accumulated after the sixth loading cycle.

(2) At the healthy state (state I), a slight irreversible increase of the resistance is observed at the unloaded phase at the beginning of each load cycle. It is influenced by the accumulation of internal microstructural cracks [Goldfeld et al. 2016a] and is correlated to the increase of the residual deflection after each load cycle. On the other hand, the electrical response of the cracked state (state III), which is characterized by a significant irreversible increase in the electrical resistance, is consistent and repeatable along the loading cycles. It is correlated to the gradual increase of the residual deflection after the formation of the macrocrack and its constant value along the unloaded phase of the next loading cycles. From the microstructural point of view, at the healthy state, the irreversible electrical response is correlated to the slight hysteretic behavior of the micromechanical response, which was attributed to internal mechanical phenomena during loading. At the cracked state, the mechanical response is governed by the presence of the macroscopic crack and no hysteresis or load relaxation is recorded (see Figures 4 and 5), which is ultimately reflected by the electrical response; see Figure 8.

(3) It is observed that the electrical resistance change due to loading is more pronounced at the healthy state. At the cracked state the correlation between the pattern of the structural response and the electrical measure is still valid, but the relative change of the resistance is much lower compared to the healthy state.

The above observations support the hypothesis of the current study that carbon rovings can sense macrostructural damage and can even distinguish between reversible and irreversible structural phenomena associated to micro- and macrocracks, respectively. This is mainly since the electrical signal is strongly affected by the microstructural mechanism of the carbon rovings within the concrete matrix. This study demonstrates these capabilities by assuming an ideal microstructural modeling of the roving within the concrete. Further investigation — which involves the effect of interfacial damage, its influence on the shear strength with respect to the fiber strength and with respect to the electrostructural response — in the context of the influence of the microscale effects on the macroscopic behavior reflected by the electrical setup define an interesting and relevant direction for additional exploration of the problem at hand.

The next section demonstrates this ability by quantitative crack identification parameters.

3.3. *Macrocrack detection.* The observations concluded from Figure 8 and Table 3 were used to determine macrocrack detection parameters. Two are related to the electrical resistance at the unloaded phase, and one is related to the relative change of the resistance and its pattern during the loading process.

3.3.1. *Macrocrack sensing by the electrical resistance at the unloaded phase.* It is clearly seen that at unloaded phases after cracking, the electrical resistance significantly increases, and this increase is

roving # ↓ load cycle →	healthy state (I)				cracking	cracked state (III)			
	2	3	4	5	6	7	8	9	10
1 (tensed)	1.007	1.069	1.294	1.313	1.448	2.557	2.315	2.422	2.124
2 (tensed)	0.923	0.982	1.239	1.462	1.636	3.040	2.658	2.663	2.426
3 (compressed)	0.760	0.872	0.995	1.066	1.210	1.871	1.728	1.867	1.576
4 (compressed)	1.215	1.505	1.612	1.712	1.786	2.428	2.353	2.497	2.217

Table 3. Initial electrical resistance change measured at the beginning of each load cycle [mΩ].

irreversible. Moreover, compared to the healthy state, this value is kept almost constant. Therefore, the study suggests to use the magnitude of the irreversible component of the electrical resistance as an indicator for the presence of macrocrack.

To correlate the electrical response to the structural response at the healthy state, it is noted that the internal microstructural phenomena lead to mechanical hysteresis of the load-deflection response (Figure 4) and to the accumulation of residual deflection after each load cycle (Figures 5 and 2). This effect is clearly reflected by the electrical response as slight increases of the resistance in the unloaded state after each load cycle is observed (Figure 8 and Table 2).

The formation of the macroscopic crack at the sixth loading cycle is indicated by a significant increase of the residual deflection and by a reduction of the relative stiffness. At the beginning of the sixth loading cycle, the residual deflection measured at the middle of the beam is 0.079 mm and the relative flexural stiffness of the beam (represented by the slope of the load deflection curve in Figure 5) is 6373 kN/m, whereas after the formation of the macrocrack the residual deflection increases to 0.234 mm and the relative flexural stiffness reduces to 3627 kN/m. This behavior is clearly reflected by the measured electrical resistance. The degradation of the structural health ultimately increases the measured electrical resistance. The average integrative electrical resistance of the four carbon rovings before the sixth loading cycle is 1.52 mΩ, whereas after this cycle the value increases to 2.47 mΩ.

In the literature, the characteristic behavior of the electrical resistance and the structural response of continuous carbon rovings was mainly reported and focused on the linear-elastic regime [Wen and Chung 1999; Wen et al. 2000; Goldfeld et al. 2016a]; the slight irreversibility that was observed in the resistance was correlated to internal microstructural phenomena. In the current study, it is seen that the formation of a macroscopic crack increases the electrical resistance significantly, and that this change is irreversible. Therefore, the resistance measured at an unloaded phase can be used as a crack indicator; it has the ability to distinguish between internal microstructural processes to external macrostructural events. In this case, initial information of the resistance of the healthy element at an unloaded phase is used as a reference value.

Without prior information of the healthy state, the resistance change at the unloaded phases from one loading cycle to another can be used by itself as a crack indicator. At the linear elastic state (cycles 1–5), the mechanical response during the loading cycles is governed by microstructural phenomena, leading to a slight increase in the measured residual deflection after each load cycle (the average increase is 14.6%; see Table 2). It is well reflected by the measured electrical resistance, which increases after each load cycle by about 20%; see Table 3. At the cracked state (cycles 7–10), the structural response is

governed by the macroscopic crack and the effect of microstructural behavior is diminished. This leads to a consistent structural response reflected by an almost constant residual deflection, and as a result, to a consistent electrical response. For the cracked state, the resistance measured at the unloaded phase between adjacent loading cycles is in the range from -13% to 8%. Therefore, even without prior data of the resistance at a reference healthy state, the relative resistance change at an unloaded phase between two adjacent loading cycles can be used as a crack indicator. That is, a small reduction in the resistance along the unloaded phase between adjacent loading cycles can lead to the conclusion that the beam has macroscopically cracked.

The electrical resistance change has a strong correlation with the micromechanical behavior and the bonding mechanism of the carbon rovings and the concrete matrix. The micromechanical behavior along the loading cycles can be explained by the telescopic pull-out mechanism in a bundled reinforcement within brittle matrix [Bartos 1987; Zhu and Bartos 1997; Bentur et al. 2010; Yardimci et al. 2011]. It is assumed that the carbon rovings are not fully bonded to the concrete matrix, meaning that only the external sleeve filaments are well bonded to the concrete matrix while the inner core ones are largely free. Due to mechanical tension loading, the external filaments formed a sleeve in which the filaments are tightly bonded to the matrix and fail, while the inner core filaments, which are not well bonded, can engage in slip and provide the stiffness to the concrete. This process is irreversible and is reflected here by the integrative electrical resistance.

Before the macroscopic crack has been formed (state I in Figures 4, 5 and 8), a gradual bonding degradation between the concrete and the carbon rovings due to loading occurs, which is mainly influenced by the external sleeve filaments. This leads to a slight irreversible increase in the resistance after each load cycle. At the damaged state (state III in Figures 4, 5 and 8), due to the formation of the macroscopic crack, the external sleeve filaments are completely degraded and broken and only the core filaments are mechanically and electrically connected, which eventually leads to a considerable irreversible increase in the measured resistance.

3.3.2. *Macrocrack sensing by an electrical resistance change along loading cycle.* The resistance profile along the loading cycle can also be used as a damage indicator. Comparing the resistance change of a similar loading profile before and after macroscopic crack formation can be used to identify the structural health state. Such results are given in Figures 9 and 10 for four couples of similar loading cycles of healthy and damaged states and for the tensed and compressed rovings, respectively. The four couples of similar loading cycles are indicated in the Figures 9 and 10 (cycles 2 and 7 are presented in Figures 9a and 10a; cycles 3 and 8 are presented in Figures 9b and 10b; cycles 4 and 9 are presented in Figures 9c and 10c; cycles 5 and 10 are presented in Figures 9d and 10d). In order to consider each load cycle independently, the resistance change and the load profile along each load cycle are plotted; the starting values of the resistance are given in Table 3. The results in Figures 9 and 10 show that the electrical readings follow the structural response for the healthy and for the damaged states. It is clearly observed that the relative change of the resistance at the damaged state is much lower than the relative change of the resistance at the healthy state. The maximum values of the relative resistance change $\Delta R/R_0$ for the eight loading cycles are given in Table 4. The maximum values of the resistance were evaluated by averaging the resistance measured along the loading phase. It is seen that for the same loading level, the relative resistance change of the healthy beam is more than three times higher than the relative resistance change

roving # ↓ load cycle →	healthy state (I)				cracked state (III)			
	2	3	4	5	7	8	9	10
1 (tensed)	0.0432	0.0497	0.0424	0.0410	0.0128	0.0152	0.0142	0.0054
2 (tensed)	0.0447	0.0532	0.0519	0.0421	0.0085	0.0115	0.0072	0.0048
3 (compressed)	0.0313	0.0393	0.0302	0.0285	0.0124	0.0123	0.0121	0.0100
4 (compressed)	0.0395	0.0408	0.0324	0.0328	0.0158	0.0143	0.0124	0.0118

Table 4. Maximum relative electrical resistance change $\Delta R / R_0$.

of the damaged beam. The low relative change in resistance after damage is mainly due to the high initial resistance at the beginning of each load cycle, which has been increased considerably due to macrocrack; see Figure 8 and Table 3. Therefore, it can be concluded that comparing the resistance change of similar loading profiles before and after cracking can be used as an indicator of macrocrack accumulation.

Here again, the electrical resistance can be directly correlated to the micromechanical behavior and the bonding mechanism of the carbon rovings and the concrete matrix. The telescopic pull-out mechanism, discussed in the previous section, is well reflected by the integrative resistance change. At the healthy state, the gradual bonding degradation of the sleeve filaments leads to the slight irreversible increase in the resistance after each load cycle and to a relatively high resistance change due to loading. At the damaged state, the external sleeve filaments are completely degraded and broken and only the core filaments, which comprises 20% of the total filaments [Bentur et al. 2010; Yardimci et al. 2011], are mechanically and electrically connected. The effect of the matrix penetration on the number of broken filaments in multifilament fiber composites has been investigated in [Yardimci et al. 2012]. This phenomenon ultimately leads to a considerable increase in the measured resistance, and as a result, the relatively small change of the resistance during loading.

4. Summary and conclusions

This paper has taken a step towards exploring the concept of using carbon/glass fiber based textile reinforcement for self-sensory TRC structural elements. Specifically, it has looked into the sensing capabilities of the carbon rovings to detect damage, which in the case of TRC structures is defined as the formation of macrocracking. It was found that the sensory textile can make a clear distinction between internal microstructural phenomena to external macroscopic structural ones. The micromechanism of the roving within the concrete matrix governed by the macrostructural response of the TRC element, which is ultimately reflected by the electrical readings.

The study offered three qualitative crack detection parameters that distinguish between the healthy state and after the formation of a macrocrack. The parameters are based on the characteristic behavior of the reversibility of the electrical response with respect to the structural behavior. It was found that at the linear-elastic regime, the slight mechanical degradation leads to a slight electronically irrecoverable response. At the damaged state, on the other hand, once the electrical resistance irreversibly increases after the formation of the macrocrack, it remains repeatable and stable. However, the relative change of the electrical resistance during the loading cycles at the cracked state is much lower than that of the
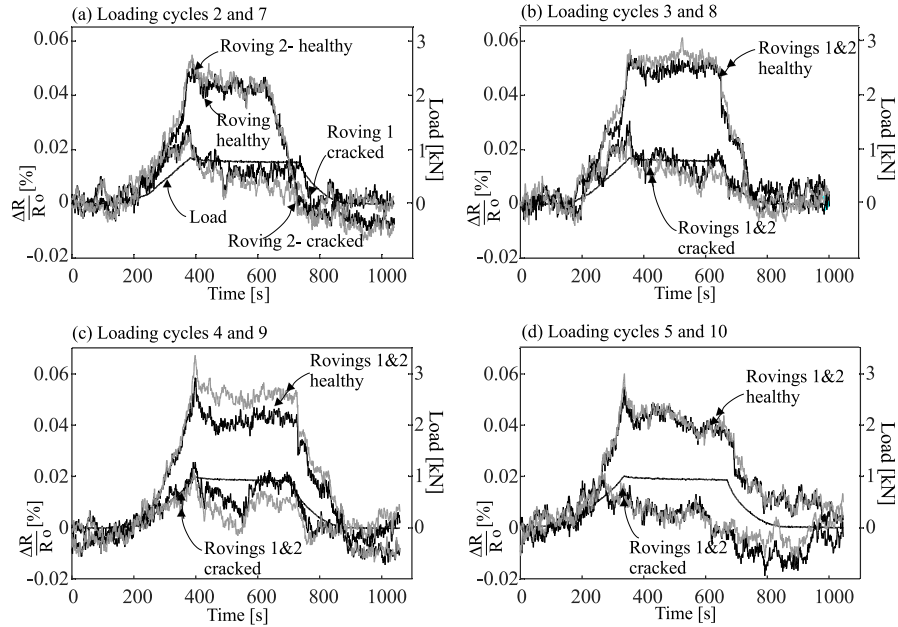
Figure 9. Resistance of the tensed carbon rovings vs. time for each loading cycle: (a) loading cycles 2 and 7; (b) loading cycles 3 and 8; (c) loading cycles 4 and 9; (d) loading cycles 5 and 10.
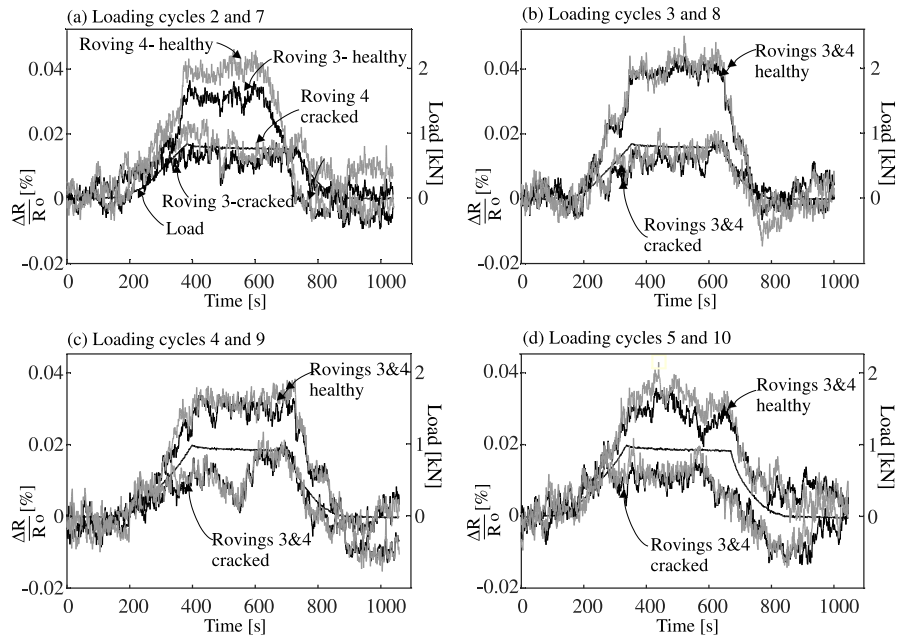

Figure 10. Resistance of the compressed carbon rovings vs. time for each loading cycle: (a) loading cycles 2 and 7; (b) loading cycles 3 and 8; (c) loading cycles 4 and 9; (d) loading cycles 5 and 10.

healthy state. It is mainly due to significant reduction in the number of filaments within the roving that continues to carry on the loading as well as to pass electrical current.

The findings of this study and the above conclusions validate the idea that the carbon/glass fiber textile can be used as reinforcement and as a damaged sensory device at the same time. The present study has focused on the ability of the textile to sense macrocracks during cyclic structural response in a TRC structural element and to distinguish between healthy to damaged state. The experimental demonstration of this aspect has taken us one step further towards the development of smart TRC structures.

Acknowledgements

References

[Angelidis et al. 2004] N. Angelidis, C. Y. Wei, and P. E. Irving, "The electrical resistance response of continuous carbon fibre composite laminates to mechanical strain", *Compos. A Appl. Sci. Manuf.* **35**:10 (2004), 1135–1147.

[Antunes et al. 2011] P. Antunes, H. Lima, N. Alberto, L. Bilro, P. Pinto, A. Costa, H. Rodrigues, J. L. Pinto, R. Nogueira, H. Varum, and P. S. André, "Optical sensors based on fiber Bragg gratings for structural health monitoring", pp. 253–295 in *New developments in sensing technology for structural health monitoring*, edited by S. C. Mukhopadhyay, Lecture Notes in Electrical Engineering **96**, Springer, Berlin, 2011.

[Banholzer and Brameshuber 2004] B. Banholzer and W. Brameshuber, "Tailoring of AR-glass filament/cement based matrix-bond: analytical and experimental techniques", pp. 1443–1452 in *Sixth RILEM Symposium on Fibre-Reinforced Concretes (BEFIB)* (Varenna, Italy, 2004), edited by M. di Prisco et al., RILEM Proceedings **Pro 039**, RILEM Publ., Bagneux, France, 2004.

[Banholzer et al. 2006] B. Banholzer, T. Brockmann, and W. Brameshuber, "Material and bonding characteristics for dimensioning and modelling of textile reinforced concrete (TRC) elements", *Mater. Struct.* **39** (2006), 749–763.

[Bartos 1987] P. Bartos, "Brittle-matrix composites reinforced with bundles of fibres", pp. 539–546 in *From materials science to construction materials engineering, II: Combining materials: design, production and properties* (Versailles, 1987), edited by J. C. Maso, Chapman and Hall, London, 1987.

[Bentur et al. 2010] A. Bentur, R. Tirosh, M. Yardimci, M. Puterman, and A. Peled, "Controlling bond characteristics by impregnation", pp. 23–33 in *Textile reinforced concrete (2nd ICTRC)* (Aachen, 2010), edited by W. Brameshuber, RILEM Proceedings **Pro 075**, RILEM Publ., Bagneux, France, 2010.

[Bontea et al. 2000] D.-M. Bontea, D. D. L. Chung, and G. C. Lee, "Damage in carbon fiber reinforced concrete, monitored by electrical resistance measurement", *Cem. Concr. Res.* **30**:4 (2000), 651–659.

[Chen and Chung 1993] P.-W. Chen and D. D. L. Chung, "Carbon fiber reinforced concrete as an electrical contact material for smart structures", *Smart Mater. Struct.* **2**:3 (1993), 181–188.

[Christner et al. 2012] C. Christner, A. Horoschenkoff, and H. Rapp, "Longitudinal and transverse strain sensitivity of embedded carbon fibre sensors", *J. Compos. Mater.* **47**:2 (2012), 155–167.

[Chung 2007] D. D. L. Chung, "Damage detection using self-sensing concepts", *Proc. Inst. Mech. Eng. G, J. Aerosp. Eng.* **221**:4 (2007), 509–520.

[Crasto and Kim 1993] A. S. Crasto and R. Y. Kim, "Using carbon fiber piezoresistivity to measure residual stresses in composites", pp. 162–173 in *Composite materials, mechanics, and processing* (Cleveland, 1993), Proceedings of the American Society for Composites Technical Conference **8**, Technomic, Lancaster, PA, 1993.

[Ding et al. 2013] Y. Ding, Z. Chen, Z. Han, Y. Zhang, and F. Pacheco-Torgal, "Nano-carbon black and carbon fiber as conductive materials for the diagnosing of the damage of concrete beam", *Constr. Build. Mater.* **43** (2013), 233–241.

[Goldfeld and Klar 2013] Y. Goldfeld and A. Klar, "Damage identification in reinforced concrete beams using spatially distributed strain measurements", *J. Struct. Eng. (ASCE)* **139**:12 (2013), art. id. 04013013.

[Goldfeld et al. 2016a] Y. Goldfeld, S. Ben-Aarosh, O. Rabinovitch, T. Quadflieg, and T. Gries, "Integrated self-monitoring of carbon based textile reinforced concrete beams under repeated loading in the un-cracked region", *Carbon* **98** (2016), 238–249.

[Goldfeld et al. 2016b] Y. Goldfeld, O. Rabinovitch, B. Fishbain, T. Quadflieg, and T. Gries, "Sensory carbon fiber based textile-reinforced concrete for smart structures", *J. Intell. Mater. Syst. Struct.* **27**:4 (2016), 469–489.

[Horoschenkoff and Christner 2012] A. Horoschenkoff and C. Christner, "Carbon fibre sensor: theory and application", pp. 357–376 in *Composites and their applications*, edited by N. Hu, InTech, Rijeka, Croatia, 2012.

[Khotiaintsev et al. 2013] S. Khotiaintsev, A. Beltrán-Hernández, J. González-Tinoco, H. Guzmán-Olguín, and G. Aguilar-Ramos, "Structural health monitoring of concrete elements with embedded arrays of optical fibers", art. id. 869513 in *Health monitoring of structural and biological systems* (San Diego, 2013), edited by T. Kundu, Proceedings of SPIE **8695**, SPIE, Bellingham, WA, 2013.

[Klar et al. 2010] A. Klar, Y. Goldfeld, and Z. Charas, "Measures for identifying cracks within reinforced concrete beams using BOTDR", art. id. 764721 in *Sensors and smart structures technologies for civil, mechanical, and aerospace systems* (San Diego, 2010), edited by M. Tomizuka, Proceedings of SPIE **7647**, SPIE, Bellingham, WA, 2010.

[Krebber et al. 2012] K. Krebber, P. Lenke, S. Liehr, N. Nöther, M. Wendt, A. Wosniok, and W. Daum, "Structural health monitoring by distributed fiber optic sensors embedded into technical textiles", *Tech. Messen* **79**:7-8 (2012), 337–347.

[Lee 2003] B. Lee, "Review of the present status of optical fiber sensors", *Opt. Fiber Tech.* **9**:2 (2003), 57–79.

[Li et al. 2004] H.-N. Li, D.-S. Li, and G.-B. Song, "Recent applications of fiber optic sensors to health monitoring in civil engineering", *Eng. Struct.* **26**:11 (2004), 1647–1657.

[Majumder et al. 2008] M. Majumder, T. K. Gangopadhyay, A. K. Chakraborty, K. Dasgupta, and D. Bhattacharya, "Fibre Bragg gratings in structural health monitoring: present status and applications", *Sens. Actuators A Phys.* **147**:1 (2008), 150–164.

[McCarter et al. 2007] W. J. McCarter, G. Starrs, T. M. Chrisp, and P. F. G. Banfill, "Activation energy and conduction in carbon fibre reinforced cement matrices", *J. Mater. Sci.* **42**:6 (2007), 2200–2203.

[Meehan et al. 2010] D. G. Meehan, S. Wang, and D. D. L. Chung, "Electrical-resistance-based sensing of impact damage in carbon fiber reinforced cement-based materials", *J. Intell. Mater. Syst. Struct.* **21**:1 (2010), 83–105.

[Mobasher et al. 2014] B. Mobasher, V. Dey, Z. Cohen, and A. Peled, "Correlation of constitutive response of hybrid textile reinforced concrete from tensile and flexural tests", *Cem. Concr. Compos.* **53** (2014), 148–161.

[Montanini et al. 2012] R. Montanini, F. De Domenico, F. Freni, N. Maugeri, and A. Recupero, "Structural health monitoring of reinforced concrete beams by means of embedded fiber Bragg grating sensors", art. id. 8421AW in *22nd International Conference on Optical Fiber Sensors (OFS2012)* (Beijing, 2012), edited by Y. Liao et al., Proceedings of SPIE **8421**, SPIE, Bellingham, WA, 2012.

[Peled et al. 2001] A. Peled, J. M. Torrents, T. O. Mason, S. P. Shah, and E. J. Garboczi, "Electrical impedance spectra to monitor damage during tensile loading of cement composites", *ACI Mater. J.* **98**:4 (2001), 313–322.

[Quadflieg et al. 2016] T. Quadflieg, O. Stolyarov, and T. Gries, "Carbon rovings as strain sensors for structural health monitoring of engineering materials and structures", *J. Strain Anal. Eng. Des.* **51**:7 (2016), 482–492.

[Reza et al. 2003] F. Reza, G. B. Batson, J. A. Yamamuro, and J. S. Lee, "Resistance changes during compression of carbon fiber cement composites", *J. Mater. Civ. Eng. (ASCE)* **15**:5 (2003), 476–483.

[Shams et al. 2014] A. Shams, M. Horstmann, and J. Hegger, "Experimental investigations on textile-reinforced concrete (TRC) sandwich sections", *Compos. Struct.* **118** (2014), 643–653.

[Silva et al. 2011] F. D. A. Silva, M. Butler, V. Mechtcherine, D. Zhu, and B. Mobasher, "Strain rate effect on the tensile behaviour of textile-reinforced concrete under static and dynamic loading", *Mater. Sci. Eng. A* **528**:3 (2011), 1727–1734.

[Stolyarov et al. 2015a] O. Stolyarov, T. Quadflieg, and T. Gries, "Effects of fabric structures on the tensile properties of warp-knitted fabrics used as concrete reinforcements", *Textile Res. J.* **85**:18 (2015), 1934–1945.

[Stolyarov et al. 2015b] O. Stolyarov, T. Quadflieg, and T. Gries, "A study of warp-knitted fabric structure parameters affecting the mechanical properties of textile-reinforced concrete", art. id. 3111–2 in *Proceedings of the 20th International Conference on Composite Materials* (Copenhagen, 2015), International Committee on Composite Materials, 2015.

[Teomete 2015] E. Teomete, "Measurement of crack length sensitivity and strain gage factor of carbon fiber reinforced cement matrix composites", *Measurement* **74** (2015), 21–30.

[Todoroki and Yoshida 2004] A. Todoroki and J. Yoshida, "Electrical resistance change of unidirectional CFRP due to applied load", *JSME Int. J. A Mech. M.* **47**:3 (2004), 357–364.

[Vaidya and Allouche 2011] S. Vaidya and E. N. Allouche, "Strain sensing of carbon fiber reinforced geopolymer concrete", *Mater. Struct.* **44**:8 (2011), 1467–1475.

[Wang and Chung 1996] X. Wang and D. D. L. Chung, "Continuous carbon fibre epoxy-matrix composite as a sensor of its own strain", *Smart Mater. Struct.* **5**:6 (1996), 796–800.

[Wang and Chung 2006] S. Wang and D. D. L. Chung, "Self-sensing of flexural strain and damage in carbon fiber polymer-matrix composite by electrical resistance measurement", *Carbon* **44**:13 (2006), 2739–2751.

[Wen and Chung 1999] S. Wen and D. D. L. Chung, "Piezoresistivity in continuous carbon fiber cement-matrix composite", *Cem. Concr. Res.* **29**:3 (1999), 445–449.

[Wen and Chung 2007] S. Wen and D. D. L. Chung, "Electrical-resistance-based damage self-sensing in carbon fiber reinforced cement", *Carbon* **45**:4 (2007), 710–716.

[Wen et al. 1999] S. Wen, S. Wang, and D. D. L. Chung, "Carbon fiber structural composites as thermistors", *Sens. Actuators A Phys.* **78**:2-3 (1999), 180–188.

[Wen et al. 2000] S. Wen, S. Wang, and D. D. L. Chung, "Piezoresistivity in continuous carbon fiber polymer-matrix and cement-matrix composites", *J. Mater. Sci.* **35**:14 (2000), 3669–3675.

[Xu et al. 2011] S. L. Xu, W. T. Yu, and S. D. Song, "Numerical simulation and experimental study on electrothermal properties of carbon/glass fiber hybrid textile reinforced concrete", *Sci. China Tech. Sci.* **54** (2011), 2421–2428.

[Yang et al. 2009] C. Yang, Z. Wu, and H. Huang, "Development of carbon fiber-based piezoresistive linear sensing technique", art. id. 72930T in *Smart sensor phenomena, technology, networks, and systems* (San Diego, 2009), edited by N. G. Meyendorf et al., Proceedings of SPIE **7293**, SPIE, Bellingham, WA, 2009.

[Yao et al. 2003] W. Yao, B. Chen, and K. Wu, "Smart behavior of carbon fiber reinforced cement-based composite", *Mater. Sci. Technol.* **19**:3 (2003), 239–242.

[Yardimci et al. 2011] M. Y. Yardimci, R. Tirosh, P. Larianovsky, M. Puterman, and R. Bentur, "Improving the bond characteristics of AR-glass strands by microstructure modification technique", *Cem. Concr. Compos.* **33**:1 (2011), 124–130.

[Yardimci et al. 2012] M. Y. Yardimci, B.-G. Kang, and W. Brameshuber, "Quantitative measurement of filament ruptures of a multi-filament AR-glass yarn embedded in concrete", *Mater. Struct.* **45**:4 (2012), 599–607.

[Zhu and Bartos 1997] W. Zhu and P. J. M. Bartos, "Assessment of interfacial microstructure and bond properties in aged GRC using a novel microindentation method", *Cem. Concr. Res.* **27**:11 (1997), 1701–1711.

YISKA GOLDFELD: yiska@technion.ac.il
Department of Civil and Environmental Engineering, Technion, Israel Institute of Technology, Haifa, Israel

TILL QUADFLIEG: till.quadflieg@ita.rwth-aachen.de
Institut fuer Textiltechnik, RWTH Aachen University, Aachen, Germany

STAV BEN-AAROSH: stavba@tx.technion.ac.il
Department of Civil and Environmental Engineering, Technion, Israel Institute of Technology, Haifa, Israel

THOMAS GRIES: thomas.gries@ita.rwth-aachen.de
Institut fuer Textiltechnik, RWTH Aachen University, Aachen, Germany

msp

JOURNAL OF MECHANICS OF MATERIALS AND STRUCTURES

msp.org/jomms

Founded by Charles R. Steele and Marie-Louise Steele

Cover photo: Wikimedia Commons